THE JOURNAL OF BIOLOGICAL CHEMISTRY VOL. 281, NO. 14, pp. 9812–9823, April 7, 2006


# Nonvisual Arrestin Oligomerization and Cellular Localization Are Regulated by Inositol Hexakisphosphate Binding*[S]

Received for publication, November 28, 2005 Published, JBC Papers in Press, January 26, 2006, DOI 10.1074/jbc.M512703200

**Shawn K. Milano[‡§], You-Me Kim[‡¶], Frank P. Stefano[‡], Jeffrey L. Benovic[‡1], and Charles Brenner[§2]**

*From the [‡]Department of Biochemistry and Molecular Biology, Thomas Jefferson University, Philadelphia, Pennsylvania 19107, [¶]The Whitehead Institute of Biomedical Research, Cambridge, Massachusetts 02142, and [§]Departments of Genetics and Biochemistry, Dartmouth Medical School, Lebanon, New Hampshire 03756*

**Interactions between arrestins and phosphoinositides have been reported to regulate multiple membrane-associated signaling and trafficking events including clathrin-mediated endocytosis and light adaptation in *Drosophila*. Arrestins have been proposed to have nuclear and cytosolic functions as well, although the ligand dependence of these functions has not been investigated. Here we characterize the structural, molecular, and cellular interactions between arrestin-2 and inositol hexakisphosphate (inositol 1,2,3,4,5,6-hexakisphosphate ($IP_6$)). The crystal structure of the arrestin-2·$IP_6$ complex was solved to 2.9 Å with crystal lattice contacts suggesting two sites on a protein monomer mediating $IP_6$ binding. Mutagenesis coupled to isothermal titration calorimetry and tritiated $IP_6$ binding assays confirmed two-site binding with a low affinity $IP_6$-binding site in the N-domain and a high affinity site in the C-domain. Native gel electrophoresis, gel filtration, and analytical ultracentrifugation demonstrated the ability of $IP_6$ to promote arrestin-2 oligomerization via the two crystallographically defined ligand-binding locations. In addition, analysis in mammalian cells revealed that arrestin-2 not only undergoes homo-oligomerization, but it can also hetero-oligomerize with arrestin-3 in a manner that depends on $IP_6$-binding sites. Mutation of either $IP_6$-binding site in arrestin-2 disrupted oligomerization while interactions with known binding partners including clathrin, AP-2, and ERK2 were maintained. Subcellular localization studies showed that arrestin-2 oligomers are primarily cytoplasmic, whereas arrestin-2 monomers displayed increased nuclear localization. Thus, by promoting cytosolic oligomerization, $IP_6$ binding is proposed to be a negative regulator of interactions of arrestin with plasma membrane and nuclear signaling proteins.**

Arrestins are a family of proteins classically known for their roles in desensitizing G protein-coupled receptors (1). They bind activated and phosphorylated receptors rendering them refractory to extracellular stimuli. Arrestins can be subdivided into two classes: visual and nonvisual. Visual arrestins (arrestin-1 and arrestin-4) are localized in retinal rod and cone cells, respectively, and regulate phototransduction. Nonvisual arrestins (arrestin-2 and arrestin-3, also called β-arrestin 1 and β-arrestin 2) are ubiquitously expressed and regulate multiple cellular processes. For example, nonvisual arrestins function as adaptor proteins interacting with endocytic components and protein kinases including phosphoinositides (2), clathrin (3), AP-2 (4, 5), and Src (6). These diverse molecules bind to arrestins forming multiprotein assemblies, which participate in clathrin-dependent endocytosis and mitogen-activated protein kinase pathways (7). Recently, however, the role of nonvisual arrestins in forming scaffolding complexes that link activated transmembrane receptors to signaling events within the cytosol and nucleus has become a central focus (7–9). These complexes, also termed signalosomes, elicit sustained intracellular signals and regulate responses such as ERK[3] nuclear translocation and cellular motility (8–10).

The expanded role of nonvisual arrestins functioning as adaptor proteins in clathrin-mediated endocytosis is intimately related to their interactions with the endocytic machinery including phosphoinositides. Phosphoinositides are recognized as important intermediates in cellular signaling and trafficking events (11). They regulate endocytosis by modulating AP-2 self-association, AP-2 binding to clathrin, and arrestin-dependent recruitment of G protein-coupled receptors into coated pits (2, 12). In addition, phosphoinositides regulate light-dependent trafficking of visual arrestins in photoreceptor cells mediating light adaptation in *Drosophila* (13). Both *Drosophila* visual arrestin and mammalian nonvisual arrestins contain a highly electropositive patch of residues located within their C-terminal domains involved in phosphoinositide binding (2, 13). Phosphoinositides such as phosphatidylinositol 4,5-bisphosphate and phosphatidylinositol 3,4,5-trisphosphate are the proposed physiological ligands for arrestins at the plasma membrane. Interestingly the soluble inositol polyphosphate inositol hexakisphosphate (inositol 1,2,3,4,5,6-hexakisphosphate ($IP_6$)) displays a higher binding affinity for nonvisual arrestins than either phosphatidylinositol 4,5-bisphosphate or phosphatidylinositol 3,4,5-trisphosphate (2). $IP_6$ is abundant in cells with concentrations ranging between 15 and 100 μM and has been proposed to participate in numerous and functionally diverse biological functions ranging from metal ion chelation to DNA repair (14, 15). Intriguingly $IP_6$ regulates both receptor endocytosis and receptor signaling. It binds with high affinity to AP-2, inhibiting clathrin coat assembly, and blocks arrestin binding to receptors and ion channels preventing signal inactivation (2, 16–19).

To understand the interactions between arrestin and $IP_6$ in greater detail we solved the crystal structure of arrestin-2 in complex with $IP_6$. The refined model at 2.9 Å provides novel structural and functional

* This work was supported by National Institutes of Health Grants GM47417 and GM068857. Isothermal titration calorimetry studies were supported by Shared Instrumentation Grant DBI 0301673, and confocal microscopy work was supported by Grant 1S10 RR019431. The costs of publication of this article were defrayed in part by the payment of page charges. This article must therefore be hereby marked "*advertisement*" in accordance with 18 U.S.C. Section 1734 solely to indicate this fact.

[S] The on-line version of this article (available at http://www.jbc.org) contains supplemental Figs. 1–3.

*The atomic coordinates and structure factors (code 1ZSH) have been deposited in the Protein Data Bank, Research Collaboratory for Structural Bioinformatics, Rutgers University, New Brunswick, NJ (http://www.rcsb.org/).*

[1] To whom correspondence may be addressed. E-mail: benovic@mail.jci.tju.edu.

[2] To whom correspondence may be addressed. E-mail: charles.brenner@dartmouth.edu.

[3] The abbreviations used are: ERK, extracellular signal-regulated kinase; $IP_6$, inositol hexakisphosphate, inositol 1,2,3,4,5,6-hexakisphosphate; ITC, isothermal titration calorimetry; ND, N-domain; CD, C-domain; NDCD, N-domain and C-domain; $IP_5$, inositol 1,3,4,5,6-pentakisphosphate; GFP, green fluorescent protein; HEK, human embryonic kidney; HA, hemagglutinin.

insights. The structural data not only define the location and the residues of arrestin-2 involved in $IP_6$ binding but also suggest a second $IP_6$-binding site with the potential for promoting $IP_6$-dependent arrestin oligomerization. The structural model was tested using biochemical and protein analytical techniques. Mutagenesis and biophysical assays established that arrestin-2 interacts with $IP_6$ at two sites and that $IP_6$ is capable of inducing arrestin-2 oligomerization via those sites. Arrestin-2 and -3 were also found to homo- and hetero-oligomerize in mammalian cells with data implicating $IP_6$ in mediating the association. Finally differences in the subcellular localization of arrestin-2 oligomers and monomers were investigated. Arrestin-2 oligomers were found to be primarily localized in the cytoplasm, whereas arrestin-2 monomers populated the nucleus. These data support a novel role for $IP_6$ in regulating receptor signaling and nuclear trafficking through arrestin oligomerization.

## EXPERIMENTAL PROCEDURES

*Arrestin Plasmid Construction*—pTrcHisB-arrestin-2, pcDNA3-arrestin-2, pcDNA3-HA-arrestin-2, pcDNA3-FLAG-arrestin-2, and arrestin-2-GFP plasmids were described previously (4, 20–22). Purified arrestin-3 was generously provided by Dr. Vsevolod Gurevich. pGEX-arrestin-2 was made by inserting arrestin-2 cDNA from the pTrcHisB-arrestin-2 plasmid into XmaI and XhoI sites of pGEX-4T-2. The arrestin-2 cDNA was amplified by PCR using 5′-cgcgcgccgggatgggcgacaaagggacgc-3′ as the sense primer and 5′-cgcgcgctcgaggggggccccc-3′ as the antisense primer. pGEX-arrestin-2 K157Q, K160Q,R161Q (ND mutant) and pcDNA3-arrestin-2 K232Q,R236Q, K250Q,K324Q,K326Q (CD mutant) were made using the QuikChange site-directed mutagenesis kit (Stratagene) according to the manufacturer's recommendations. The mutagenic primers with mutagenic codons in bold used were: K157Q, 5′-aacctggaggag**cag**atccaccagcag-3′; K160Q/R161Q, 5′-gagaagatccac**cagcag**aattctgtgcgc-3′; K232Q/R236Q, 5′-aagaagatc**cag**atctcggtg**cag**cagtatg-3′; K250Q, 5′-aacacagcccagtac**cag**tgccctgtg-3′; and K324Q/L326Q, 5′-ctacaaagtg**caa**gtg**cag**ctggtggtg-3′. pcDNA3-arrestin-2 ND and arrestin-2-GFP ND mutants were made by subcloning cDNA fragments of arrestin-2 from pGEX-arrestin-2 ND mutant into the Bsu36I/SacII and PstI/SacII sites of pcDNA3 and pEGFP-N, respectively. Arrestin-2-GFP CD and arrestin-2-GFP NDCD mutants were created by ligating the EcoRI/SacII arrestin-2 cDNA fragment from pcDNA3-arrestin-2 CD mutant into EcoRI/SacII-digested arrestin-2-GFP and arrestin-2-GFP ND mutant, respectively. pcDNA3-arrestin-2 NDCD mutant was generated by inserting the Bsu36I/SacII arrestin-2 cDNA fragment from arrestin-2-GFP NDCD mutant into the Bsu36I/SacII sites of pcDNA-arrestin-2. pcDNA3-HA-arrestin2 ND, CD, and NDCD mutants were created by subcloning the Bsu36I/SacII arrestin-2 cDNA fragment from arrestin-2-GFP ND, CD, and NDCD mutants, respectively, into Bsu36I/SacII-digested pcDNA3-HA-arrestin-2. pTrcHisB-arrestin-2 ND and NDCD mutants were constructed by inserting the Bsu36I/SacII arrestin-2 cDNA fragments from arrestin-2-GFP ND and NDCD mutants, respectively, into the Bsu36I/SacII sites of pTrcHisB-arrestin-2. pTrcHisB-arrestin-2 CD mutant was made by subcloning the EcoRI/SacII arrestin-2 cDNA fragment from pcDNA3-arrestin-2 CD mutant into EcoRI/SacII-digested pTrcHisB-arrestin-2. All constructs were verified by dideoxy dye termination sequencing.

*Expression and Purification of Arrestin-2*—Recombinant wild type arrestin-2 was expressed in BL21(DE3)-lysS bacterial cells using the pTrcHisB-arrestin-2 expression vector. Wild type arrestin-2 was purified as described previously (20). Protein purity was >99% based on SDS-PAGE and Coomassie Blue staining, and typical yields were 5–10 mg of purified arrestin-2/liter of culture. Arrestin-2 N-domain mutant (K157Q,K160Q,R161Q) and C-domain mutant (K232Q,R236Q,K250Q, K324Q,K326Q) proteins were purified according to the wild type arrestin-2 procedure, although the mutant proteins failed to interact with the SP-Sepharose high performance resin and eluted in the flow-through and wash. Protein purity was >99% based on SDS-PAGE and Coomassie Blue staining. The N-domain mutant yielded 2.6 mg of purified protein, whereas the C-domain mutant yielded 0.4 mg of purified protein/liter of culture.

*Crystallization and Data Collection*—Crystals were grown by hanging drop vapor diffusion. Drops consisted of 2 $\mu$l of protein solution (10 mg/ml in 10 mM HEPES, pH 7.2, 1 mM EDTA, and 125 mM NaCl) and 0.5 $\mu$l of 40% polypropylene glycol P 400 plus 2 $\mu$l of 150 mM magnesium formate and were equilibrated against 1 ml of 150 mM magnesium formate for 10 days. The dimensions of a typical crystal were $0.2 \times 0.1 \times 0.1$ mm. The arrestin-2 crystals were soaked for 10 min with 0.5 mM $IP_6$ in 200 mM magnesium formate; cryoprotected in 200 mM magnesium formate, 0.5 mM $IP_6$, and 25% glycerol; and flash cooled in liquid nitrogen. Diffraction data were collected at the National Synchrotron Light Source on beamline X25 at a crystal to detector distance of 220 mm with 1.5° oscillations.

*Structure Determination and Refinement*—Data were indexed and scaled using the HKL package (23). The $IP_6$-soaked arrestin-2 crystals were isomorphous to the native arrestin-2 crystals, possessing the symmetry of space group $P3_221$ and containing an arrestin monomer with one molecule of $IP_6$ in the asymmetric unit. Refinement and building were performed using the programs CNS (24) and O (25), respectively. A $F_o - F_c$ difference electron density map calculated using observed structure factor amplitudes and structure factor phases from the arrestin-2 native structure (Protein Data Bank entry 1JSY) clearly showed density for $IP_6$. $IP_6$ from Protein Data Bank entry 1GW5 was used for building into the omit density. Data from 50–2.8 Å were used to generate electron density maps to manually rebuild the model and place main chain and side chains into density. After energy minimization and grouped B-factor refinement, the final atomic model was refined to 2.9 Å with $R_{work} = 25\%$ and $R_{free} = 26\%$. The model contains 354 amino acids, 93 water molecules, 1 $IP_6$ molecule, and 1 $Mg^{2+}$. As shown in Table 1, the stereochemical parameters for the model calculated with PROCHECK (26) are reasonable and not indicative of excess geometric restraint.

*Isothermal Titration Calorimetry (ITC)*—The binding of $IP_6$ to purified arrestin-2 was investigated by ITC using a VP-ITC microcalorimeter from MicroCal. The experiments were performed in 10 mM HEPES, pH 7.2, 1 mM EDTA, and 150 mM NaCl at 10 °C. The sample cell contained 10 $\mu$M arrestin-2, and the syringe held 100 $\mu$M $IP_6$. The ligand was injected into the cell until a 1.5–2-fold molar excess of ligand to protein was achieved. In a typical experiment, 6 $\mu$l of $IP_6$ was injected into 1.43 ml of protein solution for up to 45 injections spaced 210 s apart. The heat of dilution of the ligand was subtracted from the data before fitting the curve in ORIGIN. After initial data refinement, the stoichiometry was fixed for each site to achieve the best overall fit to a two sets of sites model. The $K_d$ was determined by $K_b^{-1}$.

*Tritiated $IP_6$ Binding Assay*—The binding of $[^3H]IP_6$ to purified arrestins and its competition by unlabeled $IP_6$ were performed using a procedure described previously (16). Protein samples were incubated at 4 °C for 20 min in 100 $\mu$l of 25 mM Tris-HCl, pH 7.5, 100 mM KCl, 1 mM EDTA, 1 mM dithiothreitol, 1 mg/ml bovine $\gamma$-globulin, 0.01 $\mu$Ci of $[^3H]IP_6$, and various concentrations of unlabeled $IP_6$. The samples were then mixed with ice-cold 30% (w/v) polyethylene glycol 8000 to yield a final concentration of 20% and incubated on ice for 10 min. After centrifugation for 10 min at 4 °C at 12,000 rpm, the supernatants were

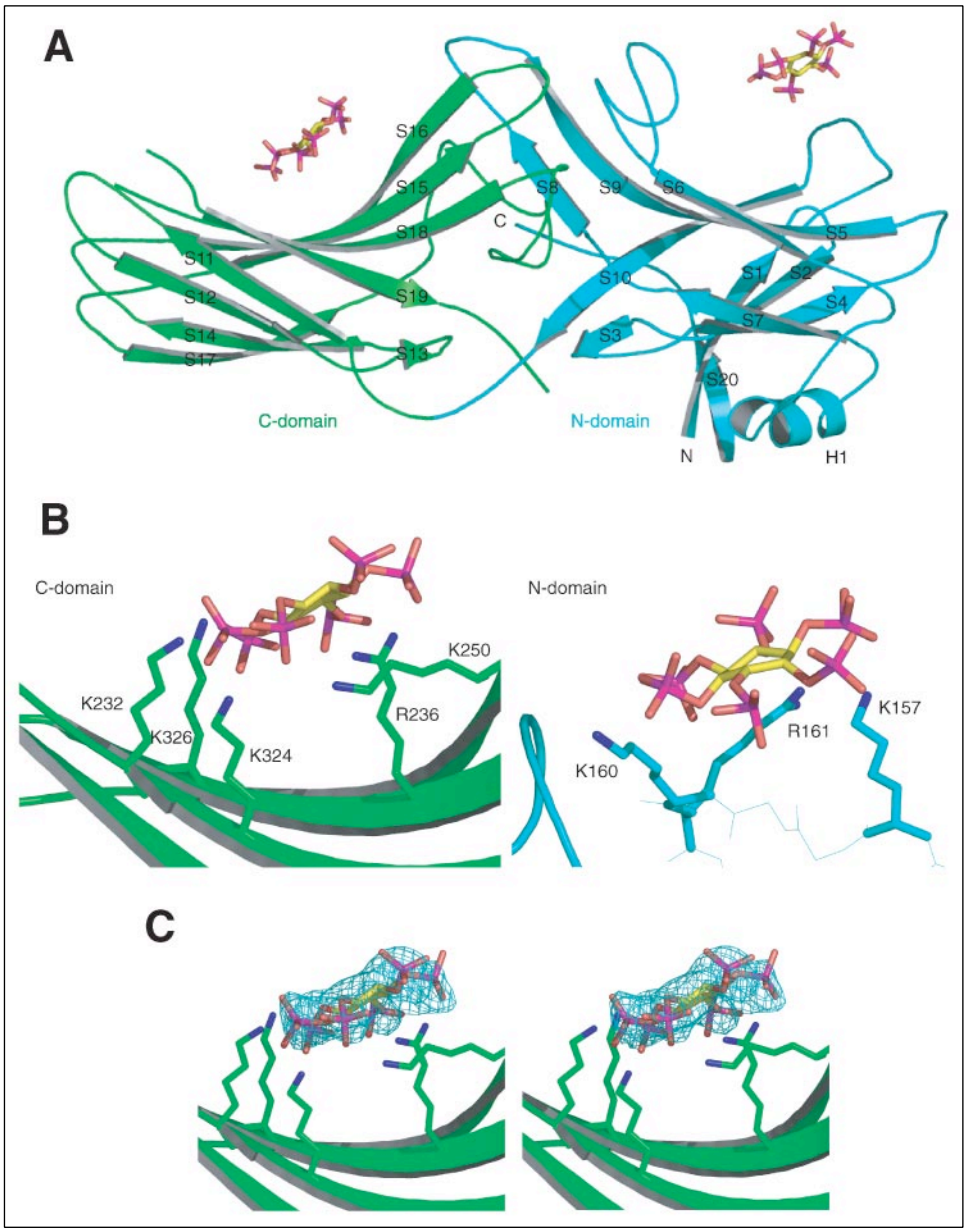


FIGURE 1. **The structure of arrestin-2·$IP_6$ complex.** *A*, ribbon diagram of the arrestin-2·$IP_6$ complex refined to 2.9 Å. $IP_6$ lies between the C-domain (*green*) and N-domain (*cyan*) of two arrestin monomers in the crystal and is shown here at both locations. *B*, arrestin-2 binding sites for $IP_6$ at the C-domain (*left*) and N-domain (*right*). Interacting residues are labeled. *C*, stereoview of the $IP_6$-binding site at the C-domain. The $F_o - F_c$ electron density map was calculated by omitting $IP_6$ and contoured to 2.7 $\sigma$. The map clearly shows density for an $IP_6$ molecule. *D*, a pictorial representation of an $IP_6$ molecule indicating possible hydrogen bonding contacts between arrestin-2 and $IP_6$. The residues on the ND interacting with $IP_6$ are labeled in *cyan*, and the interacting residues on the CD are shown in *green*. *E*, a charged surface representation of arrestin-2 showing $IP_6$ located at the N- and C-domains. The complex has been rotated by 90° toward the viewer with respect to the view in *A*. The electrostatic potential was calculated using APBS in Pymol (43) where the negative and positive potential were set to −5 and +5 kiloteslas (kT). Pymol was used to create and render the molecular images in this figure.

aspirated leaving a white pellet. The tubes were centrifuged again for 2 min, and the residual supernatant was removed. The pellet was resuspended in 200 $\mu$l of 1% SDS, transferred into scintillation vials containing 10 ml of BCS scintillation fluid (Fisher), and counted using a scintillation counter. The level of nonspecific binding was determined using 1 mM unlabeled $IP_6$.

*Gel Filtration*—A Superdex 200 HR 10/30 column was equilibrated in buffer D (10 mM HEPES, pH 7.2, 1 mM EDTA, and 150 mM NaCl) and calibrated using aldolase, bovine serum albumin, ovalbumin, and chymotrypsinogen A. Purified arrestin-2 wild type (20 $\mu$M) or a domain mutant mixture (10 $\mu$M ND + 10 $\mu$M CD) was loaded onto the column and eluted in buffer D. The column was then equilibrated in buffer D containing 50 $\mu$M $IP_6$. Purified arrestin-2 wild type (20 $\mu$M) or a domain mutant mixture (10 $\mu$M ND + 10 $\mu$M CD) incubated with $IP_6$ (50 $\mu$M) was loaded onto the column and eluted in buffer D containing 50 $\mu$M $IP_6$.

*Native Gel Electrophoresis*—Purified arrestin (10–15 $\mu$M) proteins in the presence or absence of 100 $\mu$M inositol 1,4,5-trisphosphate, inositol 1,3,4,5-tetrakisphosphate, inositol 1,3,4,6-tetrakisphosphate, inositol 1,3,4,5,6-pentakisphosphate ($IP_5$), and $IP_6$ were loaded on 5–25% gradient gels with native buffer strips and analyzed using the pHast system from Amersham Biosciences.

*Analytical Ultracentrifugation*—Analytical ultracentrifugation studies were performed on a Beckman Proteomelab XL-A with an AN-60 rotor. Sedimentation velocity runs were conducted on various concentrations of arrestin-2 in the presence or absence of $IP_6$. The samples were diluted in 10 mM HEPES, pH 7.2, 1 mM EDTA, and 150 mM NaCl (buffer C) and centrifuged at 35,000 rpm at 20 °C. Samples were also diluted in buffer C with 1 mM $MgCl_2$, which behaved similarly to buffer C alone. Protein absorbance was monitored every minute by continuous scans at either 234 or 278 nm at 0.003-cm steps. Protein partial specific volume, buffer viscosity, and buffer density were determined using the program Sednterp.[4] Scans 1–200 were analyzed using Sedfit87.

[4] D. Hayer and T. Laue, unpublished data.

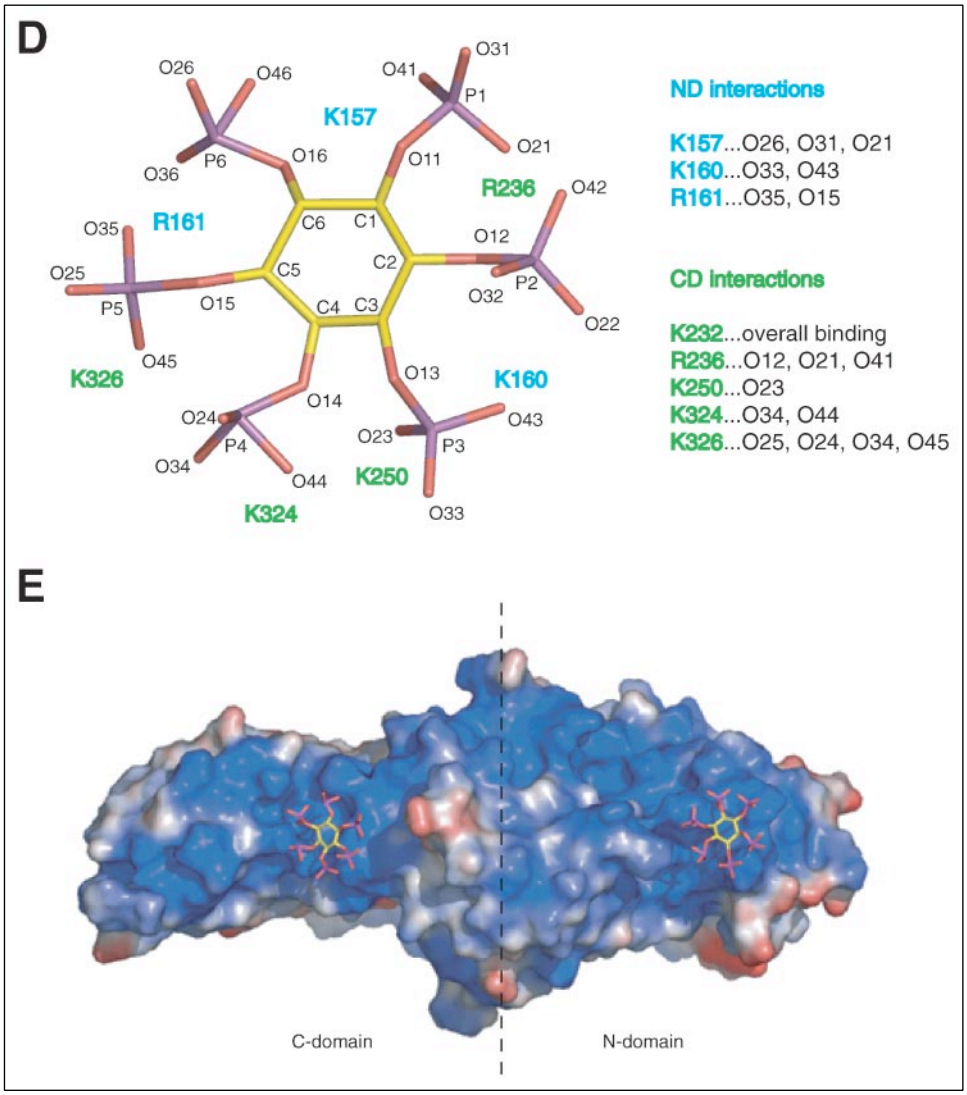


FIGURE 1—*continued*

*Cell Culture and Transient Transfection*—COS-1 and HEK293 cells were maintained in Dulbecco's modified Eagle's medium (Invitrogen) supplemented with 10% fetal bovine serum, 100 units/ml penicillin G, 100 $\mu$g/ml streptomycin sulfate, and 2 mM glutamine. The cells were grown in a humidified atmosphere of 95% air and 5% $CO_2$ at 37 °C. Transient transfection was performed with FuGENE 6 (Roche Applied Science) according to the manufacturer's recommendations.

*Analysis of Arrestin-2/3 Homo- and Heteroassociations by Co-immunoprecipitation*—COS-1 cells transiently transfected with pcDNA3-FLAG-arrestin-2 and various pcDNA3-HA-arrestin constructs were lysed in 1 ml of co-immunoprecipitation buffer containing 50 mM Tris-HCl, pH 7.5, 150 mM NaCl, 2 mM EDTA, 1% Triton X-100, and protease inhibitors. Insoluble materials were removed by centrifugation at 30,000 rpm for 20 min at 4 °C. The supernatants were incubated with 5–10 $\mu$g of polyclonal anti-HA epitope antibody (Covance) for 1 h followed by incubation with protein A-agarose for 16 h at 4 °C to immunoprecipitate the HA-tagged proteins. The immunocomplexes were washed three times in co-immunoprecipitation buffer, and samples were subjected to SDS-PAGE and Western blot analysis. FLAG-arrestin-2 was detected by monoclonal anti-FLAG (Sigma) antibody at 1:2000 dilution.

*Analysis of Arrestin-2 Interactions with Additional Proteins*—COS-1 cells transiently transfected with various pcDNA3-HA-arrestin-2 constructs were lysed in 1 ml of co-immunoprecipitation buffer. Insoluble materials were removed by centrifugation at 30,000 rpm for 20 min at 4 °C. The supernatants were incubated with 5–10 $\mu$g of polyclonal anti-HA epitope antibody (Covance) for 1 h followed by incubation with protein A-agarose for 16 h at 4 °C to immunoprecipitate the HA-tagged proteins. The immunocomplexes were washed three times in co-immunoprecipitation buffer, and samples were subjected to SDS-PAGE and Western blot analysis for clathrin using a monoclonal anti-clathrin antibody (BD Transduction Laboratories) at 1:1000 dilution, for $\beta_2$-adaptin using a monoclonal anti-$\beta_2$-adaptin antibody (BD Transduction Laboratories) at 1:1000 dilution, and for ERK2 using a monoclonal anti-ERK2 antibody (Santa Cruz Biotechnology) at 1:500 dilution.

*Subcellular Localization Analysis*—HEK293 cells were transiently transfected with various arrestin-2-GFP constructs in a 6-well plate. Twenty-four hours later the cells were split and plated onto another 6-well plate containing glass coverslips. After another 24 h the cells (~50–60% confluent) were fixed in 3.7% formaldehyde for 15 min. 4′,6-Diamidino-2-phenylindole (0.1 $\mu$g/ml) was then added to the fixed cells for 5 min to stain the nucleus. Coverslips were mounted onto glass slides containing 10 $\mu$l of Prolong Anti-Fade reagent (Molecular Probes). The slides were visualized on an Olympus BX-61 microscope with an ORCA-ER (Hamamatsu, Bridgewater, NJ) cooled charge-coupled device camera controlled by Slidebook version 4.0 (Intelligent

**TABLE 1**

**Crystallographic data and refinement statistics**

Data in parentheses refer to the highest resolution shell. r.m.s., root mean square.

| | |
|---|---|
| **Data collection** | |
| Space group | $P3_221$ |
| Cell dimensions | |
| *a*, *c* (Å) | 78.88, 158.38 |
| Resolution (Å) | 50–2.8 |
| $R_{sym}$ (%)[a] | 4.7 (30.1) |
| $I/\sigma$ | 17.8 |
| Completeness (%) | 99.7 (97.7) |
| Redundancy[b] | 16.9 |
| **Refinement** | |
| Resolution (Å) | 2.9 |
| Work reflections | 12,003 |
| Test reflections | 917 |
| $R_{work}/R_{free}$ (%)[c,d] | 25.0/26.4 |
| Number of atoms | |
| Protein | 2,805 |
| Non-protein | 130 |
| Average B-factor | |
| Protein (Å) | 53.3 |
| Non-protein (Å) | 73.3 |
| r.m.s. deviations | |
| Bond lengths (Å) | 0.013 |
| Bond angles (°) | 1.8 |

[a] $R_{sym} = \Sigma|I - \langle I\rangle|/\Sigma\langle I\rangle$ in which $I$ is a measured intensity and $\langle I\rangle$ is the average intensity from multiple measurements of symmetry-related reflections.
[b] Redundancy = total number of observations/unique reflections.
[c] $R_{work} = \Sigma|F_{obs} - F_{calc}|/\Sigma F_{obs}$.
[d] $R_{free}$ was calculated as for $R_{work}$ using test reflections excluded from atomic refinement.

Imaging Innovations, Denver, CO) and on a Zeiss LSM 510 META confocal laser scanning microscope system.

## RESULTS

*Arrestin-2 Has Two Crystallographically Defined $IP_6$-binding Sites*—On the basis of our crystal structure of arrestin-2, we hypothesized that residues Lys-232, Arg-236, Lys-250, Lys-324, and Lys-326 would be involved in interactions with phosphoinositide head groups (20). To test this model and to determine how arrestin-2 binds to the abundant cytosolic inositol polyphosphate $IP_6$, we soaked $IP_6$ into arrestin-2 crystals and solved the liganded structure (Fig. 1*A* and Table 1). Arrestin-2 crystals have a monomer in the asymmetric unit and a well refined binding site for $IP_6$ in the predicted location (Fig. 1*C*). Indeed $IP_6$ binds to a highly electropositive region within the C-terminal domain of arrestin-2 with Lys-232, Arg-236, Lys-250, Lys-324, and Lys-326 contributing to the overall binding of the ligand (Fig. 1, *B* and *E*). As in the case of clathrin assembly lymphoid myeloid leukemia protein (CALM) and $\alpha$-adaptin, $IP_6$ binds to arrestin-2 through interactions at the polar termini of Lys and Arg side chains rather than binding in a pocket or groove (27, 28). Residues Lys-232, Arg-236, and Lys-250 correspond to the residues in arrestin-3 (Lys-233, Arg-237, and Lys-251) that were previously shown to bind phosphoinositides and regulate G protein-coupled receptor trafficking (2). The crystal structure shows two additional basic residues with binding contacts, Lys-324 and Lys-326. In fact, Lys-326 along with Arg-236 can form the greatest number of hydrogen bonds with $IP_6$. Lys-324 is in a position to make two hydrogen bond contacts with $IP_6$ while Lys-250 makes one apparent hydrogen bond. Although Lys-232 appears to have the weakest interaction with the ligand, it contributes to the overall electropositive surface (Fig. 1, *D* and *E*). A superposition of $IP_6$-bound and unbound arrestin-2 structures shows no significant global conformational changes or rearrangements resulting from ligand binding (supplemental Fig. 1A). A close-up view of the $IP_6$-binding domains, however, shows side chain differences. The side chains of the arrestin-2·$IP_6$-bound structure have moved toward the ligand, especially Arg-236 and Lys-326 in the C-domain and Arg-161 in the N-domain (supplemental Fig. 1B).

$IP_6$ is sandwiched between neighboring arrestin monomers in the crystal lattice. Arrestin-2 consists of 20 $\beta$-strands and a single $\alpha$-helix arranged into what has been termed the N-domain and the C-domain (Fig. 1*A*) (20, 29, 30). These two domains are separated by a short linker formed by residues 174–181 (20). $IP_6$ interacts with the C-domain of one arrestin-2 monomer as described above and the N-domain of a symmetry mate. In fact, the two monomers appear to chelate the ligand. The electrostatic surface of the N-domain, like the C-domain, is also highly positive (Fig. 1*E*). The amino acids in the N-domain interacting with $IP_6$ are Lys-157, Lys-160, and Arg-161 (Fig. 1*B*). Lys-157 is in position to make three contacts with $IP_6$ while Lys-160 and Arg-161 can each make two (Fig. 1*D*). Thus, the crystal structure of arrestin-2 with $IP_6$ predicts a second $IP_6$-binding site.

*Arrestin-2 Has a High Affinity and a Low Affinity Binding Site for $IP_6$*—Based upon the co-crystal structure, we investigated whether arrestin-2 contains two binding sites for $IP_6$. ITC and tritiated $IP_6$ binding assays were used to evaluate the binding of $IP_6$ to purified, wild type arrrestin-2. The ITC data fit a two-site model with a $K_d$ of 0.04 ± 0.02 $\mu$M for the high affinity site and a $K_d$ of 2.6 ± 0.2 $\mu$M for the low affinity site (Fig. 2*A*). The tritiated $IP_6$ binding data also fit well to a two-site binding model. As shown in Fig. 2*B*, 4 pmol of wild type arrestin-2 (40 nM) bound ~8 pmol of $IP_6$. Scatchard analysis indicated that the $K_d$ of the high affinity site was 0.05 ± 0.01 $\mu$M while the $K_d$ of the low affinity site was calculated to be 0.9 ± 0.2 $\mu$M.

To further test the binding of $IP_6$ to purified arrestin-2 and to determine whether crystallographically defined amino acids mediate $IP_6$ binding, point mutations in the N- and C-domains of arrestin-2 were introduced to inhibit $IP_6$ binding while allowing the two surfaces to remain polar (supplemental Fig. 2). The substitutions made in the N-domain were K157Q,K160Q,R161Q (ND mutant) while those in the C-domain were K232Q,R236Q,K250Q,K324Q,K326Q (CD mutant). Arrestin-2 ND and CD mutants were evaluated for $IP_6$ binding using the tritiated $IP_6$ assay (Fig. 2*C*). The data show that the low affinity site is located on the N-domain because the CD mutant contained a single binding site with a $K_d$ of 1.1 ± 0.1 $\mu$M. Similarly the high affinity site is located on the C-domain because the ND mutant contained a single binding site with a $K_d$ of 0.26 ± 0.03 $\mu$M. These data establish that arrestin-2 ND and CD mutants bind $IP_6$ with a 1:1 stoichiometry, whereas native arrestin-2 at 40 nM binds two $IP_6$ equivalents with the high affinity site in the C-domain.

*Inositol Hexakisphosphate Induces Arrestin-2 Oligomerization*—The manner in which $IP_6$ interacts with arrestin-2 in the crystal lattice suggests the potential to form an $IP_6$-dependent arrestin-2 oligomer. The crystal structure shows $IP_6$ interacting with the N-domain of one arrestin molecule and the C-domain of another molecule (Fig. 3*A*). The tritiated $IP_6$ binding data are consistent with exact locations of two crystallographically defined $IP_6$-binding sites but do not establish whether $IP_6$ binding promotes arrestin oligomerization. The calorimetric data, however, requiring an initial concentration of 10 $\mu$M protein in addition to measuring free $IP_6$ binding to arrestin may also be recording the heat liberated by arrestin-2·$IP_6$ binding to another arrestin-2 molecule.

To test the hypothesis that $IP_6$ promotes arrestin-2 oligomerization in a manner seen in the crystal structure (Fig. 3*A*), native gel electrophoresis, size exclusion chromatography, and analytical ultracentrifugation techniques were used. Native gel studies showed an $IP_6$-dependent shift in gel mobility for wild type arrestin-2 (Fig. 3*B*) consistent with oligomerization. This assay, with arrestin-2 at 10 $\mu$M and $IP_6$ at 100 $\mu$M, was used to test whether oligomerization depends not only on the crystallographically identified amino acids but on the presence of an intact N-domain and C-domain in an arrestin preparation. According to the

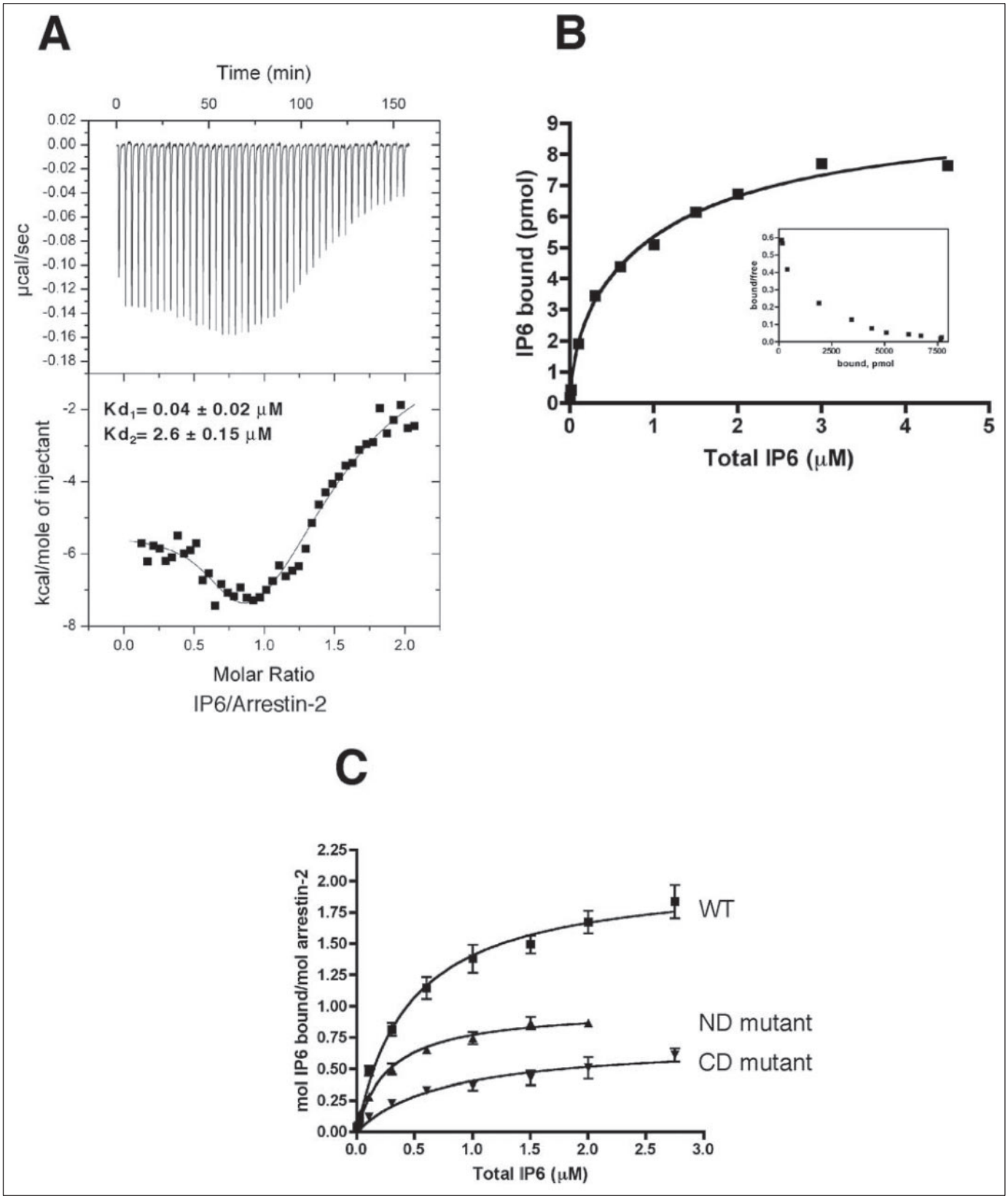


FIGURE 2. **Arrestin-2 has two $IP_6$-binding sites.** *A*, ITC measurements showing arrestin-2·$IP_6$ fitting a two-site model. The data reveal a high affinity site (0.04 $\mu$M) and a low affinity site (2.6 $\mu$M). The stoichiometry for each site is 0.74 ± 0.03, while the enthalpy for the high and low affinity sites are −4.8 ± 0.7 and −10.0 ± 1.9 kcal $mol^{-1}$, respectively. Binding constants ($K_d$), stoichiometry (*N*), and enthalpy ($\Delta H$) reflect mean and S.D. from three independent experiments. *B*, inositol polyphosphate binding assay demonstrating the stoichiometry of $IP_6$ to arrestin-2 is 2:1; ~8 pmol of [$^3$H]$IP_6$ is bound to 4 pmol of arrestin-2 assayed in the experiment. *Inset*, Scatchard analysis. *C*, stoichiometric binding analysis of [$^3$H]$IP_6$ to wild type (*WT*) and mutant arrestin-2 proteins as indicated in the graph. *Error bars* reflect mean and S.D. from three independent experiments.

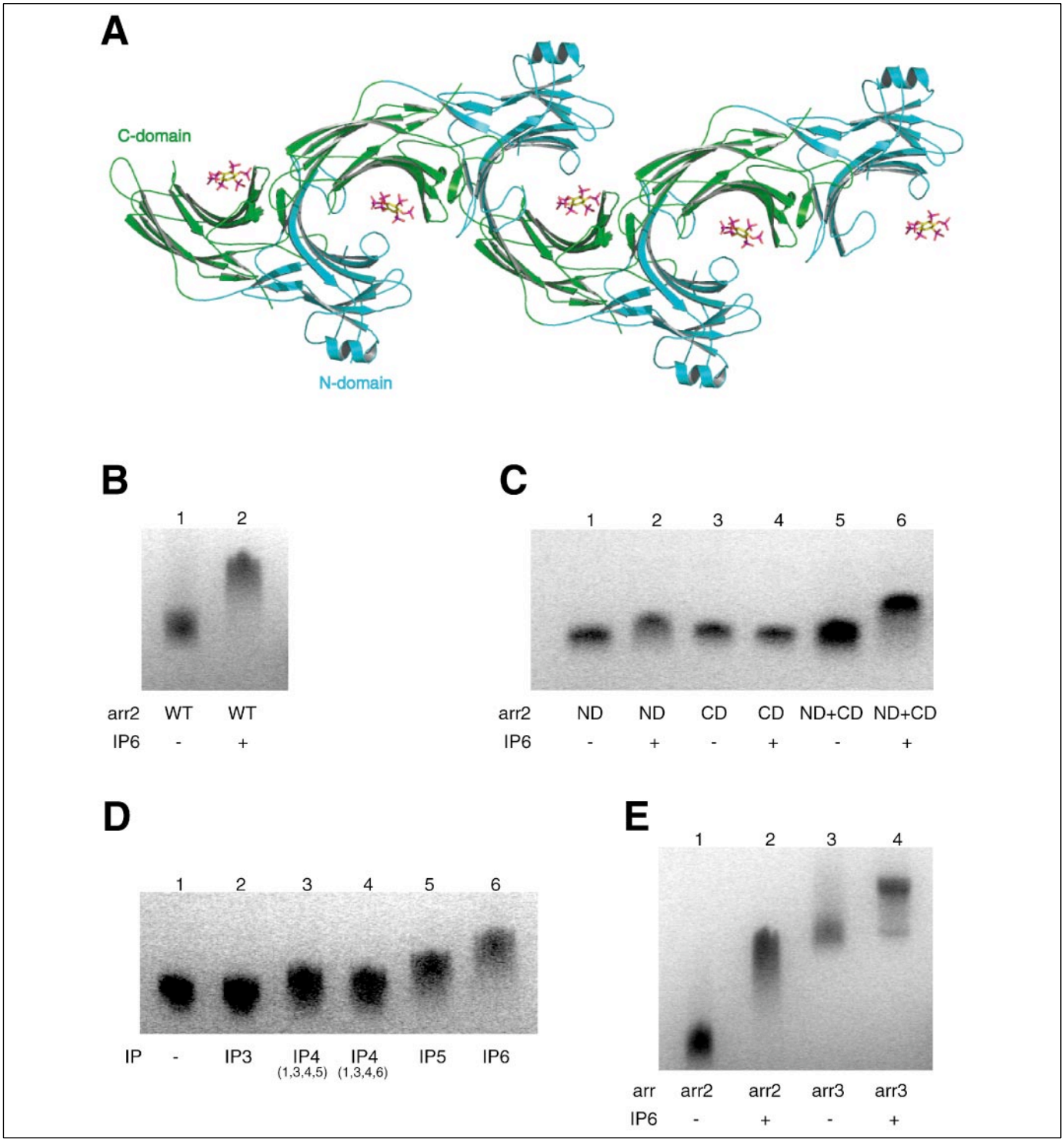


FIGURE 3. **$IP_6$-induced arrestin association.** *A*, arrestin-2 self-association complex depicted in the crystal lattice. $IP_6$ is in a position to bridge the ND of one monomer with the CD of another monomer. *B*, arrestin-2 (10 $\mu$M) gel migration in the presence of $IP_6$ (100 $\mu$M). *C*, gel migration of arrestin-2 domain mutants in the presence of $IP_6$ (100 $\mu$M). Purified mutant arrestin-2 proteins (10 $\mu$M) were analyzed as indicated in the figure. *D*, wild type arrestin-2 (10 $\mu$M) gel migration in the presence of various inositol phosphates (100 $\mu$M). *Lane 2*, inositol 1,4,5-trisphosphate (*IP3*); *lane 3*, inositol 1,3,4,5-tetrakisphosphate (*IP4 (1,3,4,5)*); *lane 4*, inositol 1,3,4,6-tetrakisphosphate (*IP4 (1,3,4,6)*); *lane 5*, $IP_5$; *lane 6*, $IP_6$. *E*, wild type arrestin-2 and -3 (15 $\mu$M) gel migration in the presence of $IP_6$ (100 $\mu$M). *arr2*, arrestin-2; *arr3*, arrestin-3; *WT*, wild type.

crystal lattice model, a preparation of ND or CD mutant proteins should independently fail to oligomerize, whereas a combination of the two proteins should *trans*-complement each other and self-associate. As shown in Fig. 3*C*, this was exactly the case. The arrestin-2 ND mutant, which maintains the high affinity binding site, displayed a slight gel shift in the presence of $IP_6$, consistent with co-migration of arrestin-2 with $IP_6$ in the native gel, but unlike the large mobility shift seen for wild type arrestin-2. Mobility of the CD mutant, lacking the high affinity binding site, was unaffected by the ligand (Fig. 3*C*). Moreover when the ND and CD mutants were mixed together (Fig. 3*C*, *lanes 5* and *6*) a substantial, $IP_6$-dependent mobility shift was observed, supporting the $IP_6$-mediated arrestin-2 architecture shown in Fig. 3*A*.

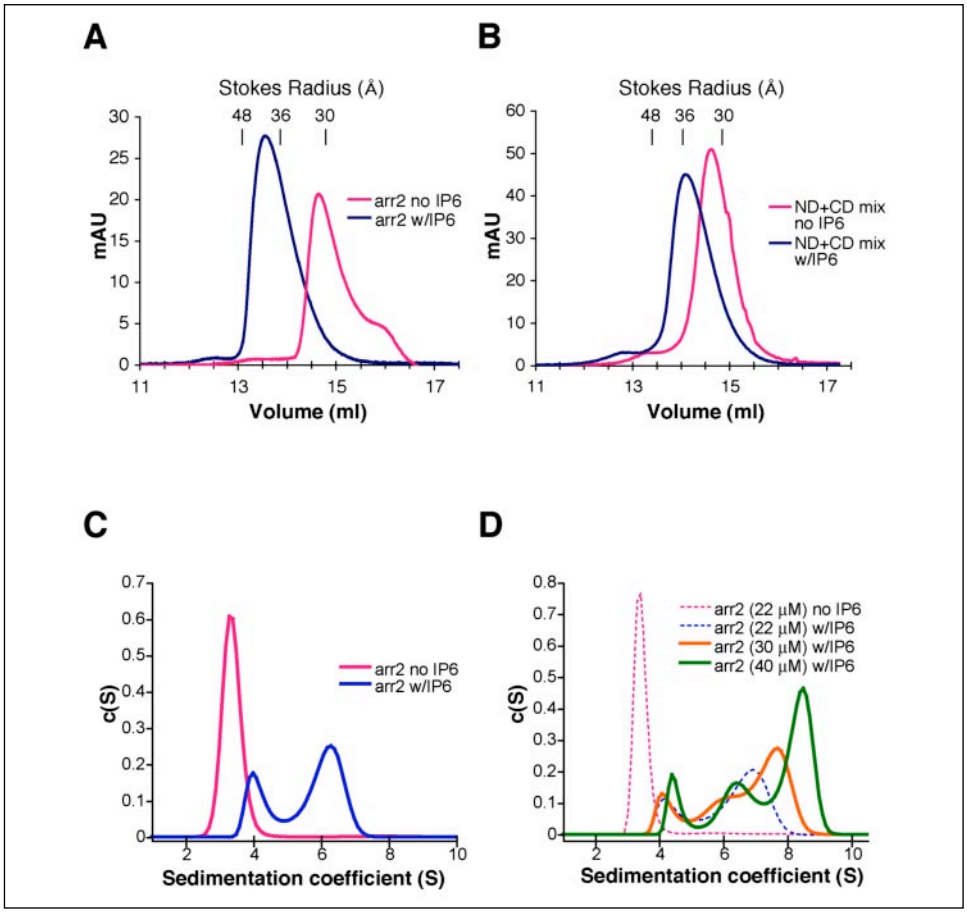


FIGURE 4. **Arrestin-2 forms oligomers in the presence of $IP_6$.** *A* and *B*, gel filtration chromatography of arrestin-2 in the absence (*pink*) and presence (*blue*) of $IP_6$. In *B*, arrestin-2 ND and CD mutants (*ND+CD mix*) were incubated together before analysis. Stokes radii for the protein standards aldolase (48 Å), bovine serum albumin (36 Å), and ovalbumin (30 Å) are indicated. The molecular masses for aldolase, bovine serum albumin, and ovalbumin are 158, 68, and 43 kDa, respectively. *C*, $IP_6$-induced arrestin-2 wild type oligomerization determined by analytical ultracentrifugation: velocity sedimentation experiment showing arrestin-2 alone (22 $\mu$M) in *pink* and arrestin-2 incubated with $IP_6$ (100 $\mu$M) in *blue*. *D*, velocity sedimentation data showing the oligomeric state of arrestin-2 with or without $IP_6$ (100 $\mu$M) as the concentration of arrestin-2 is increased. The data plotted in *pink* and *blue* indicate experiments performed under the same conditions as in *C*. The data plotted in *orange* (30 $\mu$M arrestin) and *green* (40 $\mu$M arrestin) show additional species of arrestin-2 forming as the arrestin-2 concentration is increased in the presence of $IP_6$. Velocity sedimentation data were evaluated using a continuous *c*(*S*) distribution model. *arr2*, arrestin-2; *mAU*, milliabsorbance units; *w/*, with.

Native gel electrophoresis was also utilized to explore the ligand specificity of arrestin-2 mobility. As shown in Fig. 3*D*, $IP_5$ induced a measurable, although lesser mobility shift than $IP_6$, whereas no significant shift was evident for inositol 1,4,5-trisphosphate, inositol 1,3,4,5-tetrakisphosphate, or inositol 1,3,4,6-tetrakisphosphate. These data demonstrate the importance of having a highly phosphorylated inositol ring to promote arrestin oligomerization and are consistent with the observation that residues in the N-domain and the C-domain recognize phosphate oxygens on all six phosphates.

Because the amino acids of arrestin-2 that interact with $IP_6$ are completely conserved in arrestin-3 (supplemental Fig. 2), we also evaluated whether $IP_6$ induced a mobility shift of arrestin-3. Indeed arrestin-3 displayed a significant gel shift in the presence of $IP_6$ establishing that $IP_6$ induces oligomerization of arrestin-3 *in vitro* (Fig. 3*E*).

The size of arrestin-2 treated with $IP_6$ was further characterized by gel filtration. Unliganded arrestin-2 at 20 $\mu$M protein concentration migrated with a calculated Stokes radius of 32.2 Å between globular protein standards of 43 kDa (ovalbumin) and 68 kDa (bovine serum albumin) consistent with a 47.1-kDa monomer (Fig. 4*A*). When incubated with $IP_6$, arrestin-2 ran much faster in the gel with a calculated Stokes radius of 41.8 Å, migrating between bovine serum albumin and aldolase (158 kDa). The rapidly migrating arrestin-2 fraction run on a native gel recapitulated the arrestin-2·$IP_6$ gel shift seen in Fig. 3*B* (data not shown). Consistent with the $IP_6$-dependent native gel shift of the ND mutant plus CD mutant seen in Fig. 3*C*, 10 $\mu$M ND mutant plus 10 $\mu$M CD mutant ran with the same Stokes radius as wild type arrestin-2 in the absence of $IP_6$, whereas $IP_6$ shifted all of the protein to a faster migrating form (Fig. 4*B*). However, the *trans*-complementation of oligomer formation by $IP_6$-mediated binding to the ND and CD mutant mixture was not complete. Whereas wild type arrestin-2·$IP_6$ migrated between bovine serum albumin and aldolase, the ND·CD·$IP_6$ complex shifted the mobility to approximately that of bovine serum albumin with a calculated Stokes radius of 35.8 Å. The crystal lattice model of $IP_6$-mediated arrestin polymerization makes three specific predictions. First, $IP_6$ should fail to mediate homodimerization of an ND mutant or a CD mutant because $IP_6$ bridges the contacts of a C-domain of one monomer to a N-domain of another monomer. Second, $IP_6$ should mediate dimerization of a ND mutant with a CD mutant. Third, whereas $IP_6$ addition to wild type arrestin-2 should allow formation of an oligomer larger than a dimer, $IP_6$ addition to a mixture of ND plus CD should only allow dimer formation. Gel filtration data were entirely consistent with these predictions and indicate that the 32.2-Å radial form is a monomer, whereas the ND·CD·$IP_6$ form of 35.8 Å is a dimer, and the wild type arrestin-2·$IP_6$ complex with a Stokes radius of 41.8 Å is larger than a dimer.

Analytical ultracentrifugation also revealed an $IP_6$-induced oligomerization of arrestin-2. The addition of $IP_6$ to arrestin-2 resulted in a shift in the sedimentation coefficient (*S*) when compared with arrestin-2 alone (Fig. 4*C*). The sedimentation coefficient for arrestin-2 alone ranged from 2.3 to 4.65, corresponding to a molecular mass of ~45 kDa. When $IP_6$ was incubated with arrestin-2, two populations of *S* values were apparent ranging from 3.32 to 4.89 and 4.89 to 7.48, respectively. The molecular mass for the smaller population corresponds to ~47 kDa, similar to the molecular mass of arrestin-2 alone. The higher molecular mass species corresponds to ~93 kDa, demonstrating an $IP_6$-dependent oligomer. Interestingly the data indicate that as the arrestin-2 concentration is increased, the sedimentation coefficient continually becomes greater forming multiple species of arrestin-2 (Fig.

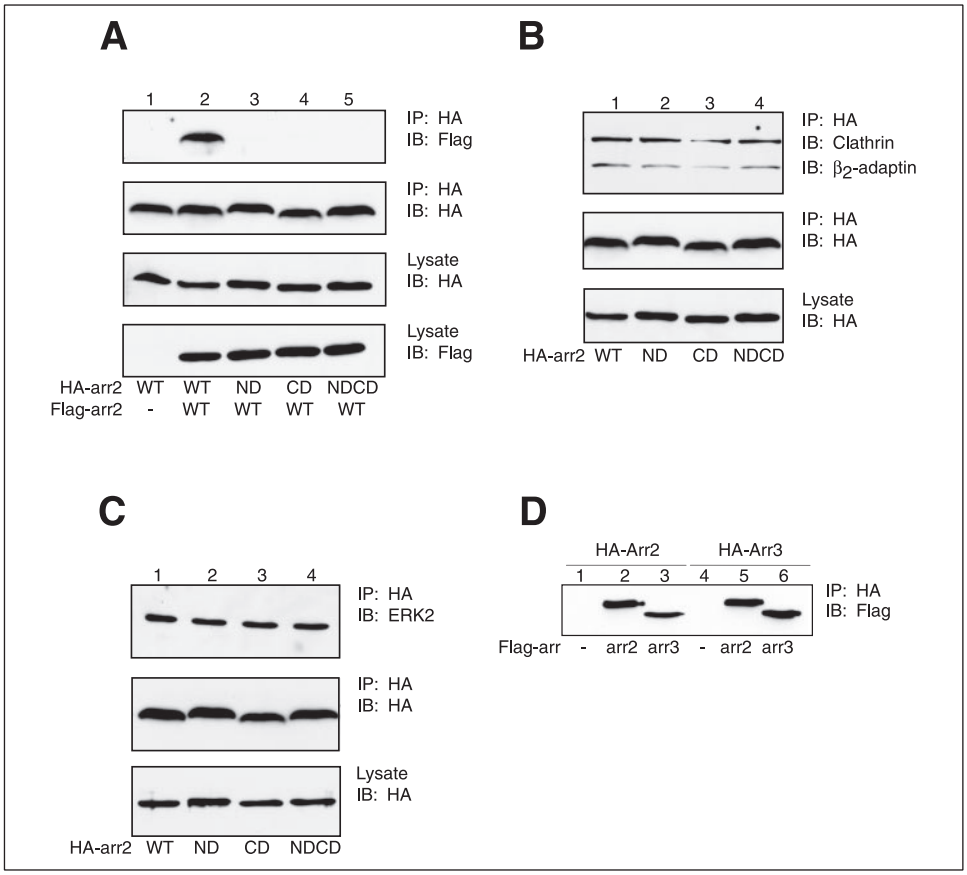


FIGURE 5. **Arrestin-2 and -3 can homo- and heteroassociate in COS-1 cells.** *A*, co-immunoprecipitation experiment showing wild type arrestin-2 associating with itself. Mutation of the two crystallographically defined $IP_6$-binding sites on arrestin-2, either independently or combined, disrupts self-association. HA-tagged wild type and mutant arrestin-2 proteins were overexpressed in COS-1 cells with or without FLAG-tagged wild type arrestin-2. HA-arrestins were immunoprecipitated and blotted for FLAG-arrestin-2. Immunoprecipitate (*IP*) and lysate expression levels are shown. *B* and *C*, co-immunoprecipitation experiments showing arrestin-2 mutants effectively interacting with known binding partners. HA-tagged wild type and mutant arrestin-2 proteins were overexpressed in COS-1 cells. HA-arrestins were immunoprecipitated and blotted for clathrin, $\beta_2$-adaptin, and ERK2. Immunoprecipitate and lysate expression levels are shown. *D*, co-immunoprecipitation experiment showing that wild type arrestin-2 and -3 can homo- and heteroassociate. HA-tagged arrestin-2 and -3 proteins were overexpressed in COS-1 cells with or without FLAG-tagged arrestin-2 or -3. HA-arrestins were immunoprecipitated and blotted for FLAG-arrestins. − indicates mock transfection. *IB*, immunoblot; *WT*, wild type; *arr2*, arrestin-2; *arr3*, arrestin-3.

4*D*). Overall the addition of $IP_6$ results in a ligand-dependent, mass action oligomerization of arrestin-2.

Because a substantial shift in the native gel electrophoresis assay required both $IP_6$-binding sites as shown in Fig. 3*B* (*lane 2*) and Fig. 3*C* (*lane 6*), we propose that $IP_6$-dependent oligomerization requires that $IP_6$ be sandwiched between an intact N-terminal domain site and an intact C-terminal domain site as seen in the crystal structure. Mutation of either $IP_6$-binding site disrupts homo-oligomerization because the oligomer appears to require both sites to form (Fig. 3*C*, *lanes 2* and *4*).

*Arrestins Undergo Homo- and Hetero-oligomerization in Cells*—Arrestin-2 and arrestin-3 were recently shown to homo- and hetero-oligomerize in cells at expression levels that approximate native levels (31). To determine whether arrestin-2 oligomerization in cells depends on $IP_6$ binding, we performed co-precipitation experiments using differentially tagged arrestins expressed in COS-1 cells. FLAG-tagged arrestin-2 effectively co-precipitated with HA-tagged arrestin-2 when transiently co-expressed in COS-1 cells (Fig. 5*A*, *lane 2*). Mutation of the N-domain binding residues, the C-domain binding residues, or a combination of both sets of residues effectively blocked co-precipitation (Fig. 5*A*, *lanes 3–5*).

*In vitro* we observed the failure of ND or CD mutant proteins to form oligomers. However, co-incubation of ND and CD mutants formed a ND·$IP_6$·CD species consistent with dimer formation, whereas wild type arrestin-2·$IP_6$ formed a complex larger than a dimer. In the cell-based assay, according to the lattice model, an ND or CD mutant would be capable of either forming a dimer with wild type arrestin-2 or effectively capping the terminus of a wild type polymer because only one of its domains could mediate an $IP_6$ interaction. Failure to detect FLAG-tagged ND or CD mutants by immunoprecipitating with HA-tagged arrestin-2 is consistent with effective exclusion of single domain mutants from wild type arrestin-2 polymers.

An alternative explanation for the exclusion of ND and CD mutants from HA-arrestin-2 oligomers is that mutations of the $IP_6$-binding sites may have caused an unanticipated protein destabilization or conformational change. Accordingly we tested whether the arrestin-2 mutants could interact with several known binding partners. The mutants, although unable to self-associate, were still able to interact effectively with proteins implicated in trafficking (clathrin and $\beta_2$-adaptin) and signaling (ERK2) (Fig. 5, *B* and *C*) (4, 32, 33). These data indicate that clathrin, $\beta_2$-adaptin, and ERK2 binding are independent of the $IP_6$-binding sites. Additionally because ND and CD mutants can form dimers *in vitro* but were not detected to form oligomers by co-immunoprecipitation with wild type in cells, we suggest that much of wild type arrestin-2 may be preferentially self-associating as a larger polymer.

Because our studies suggested that arrestin-3 also could undergo $IP_6$-promoted oligomerization (Fig. 3*E*), we next evaluated whether arrestin-3 homo-oligomerizes in cells and whether arrestin-2 and -3 were capable of undergoing hetero-oligomerization. HA-tagged arrestin-2 and -3 with or without FLAG-tagged arrestin-2 or -3 were transiently expressed in COS-1 cells. HA-arrestin-2 and -3 were immunoprecipitated and blotted for FLAG-tagged arrestins. As shown in Fig. 5*D*, both FLAG-arrestin-2 and -3 co-precipitated with HA-arrestin-2 demonstrating that arrestin-2 can associate with itself or with arrestin-3 in cells. Similarly HA-arrestin-3 forms a complex with both FLAG-arrestin-2 and -3. Thus, as reported elsewhere, both arrestin-2 and arrestin-3 homo- and hetero-oligomerize in cells (31).

*Monomeric $IP_6$ Binding Mutants of Arrestin-2 Are More Nuclear*—Wild type arrestin is an $IP_6$-dependent multimer *in vitro* and oligomeric in cells in a manner that depends on the amino acids for binding $IP_6$ at two crystallographically defined locations. To test whether failure to multimerize might lead to an altered subcellular distribution, we fused wild type and mutant

arrestin-2 constructs to GFP and studied their localization in transfected HEK293 cells by confocal and conventional fluorescence microscopy. In these unstimulated cells, wild type arrestin-2 was predominately localized in the cytoplasm, whereas the mutants were more concentrated in the nucleus (Fig. 6). These data suggest that $IP_6$ binding and/or oligomerization of arrestin-2 may present a barrier to nuclear localization. Although loss of $IP_6$ binding could be proposed to promote interactions with the nuclear transport machinery by revealing eight basic amino acids, we do not propose such a model because the NDCD mutant, lacking these amino acids, is more nuclear than is the wild type protein. Rather we propose that the arrestin-2 structure contains $IP_6$-binding sites that promote cellular oligomerization and that multimers are disadvantaged in nuclear localization.

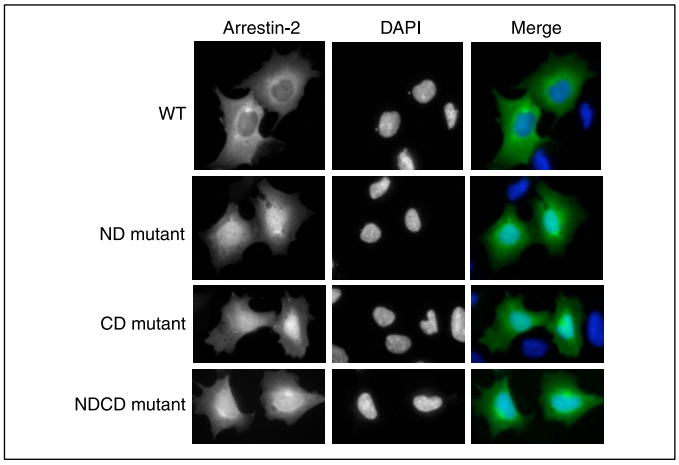


FIGURE 6. **Arrestin-2 oligomers are deficient in nuclear transport.** HEK293 cells were transiently transfected with either wild type (*WT*) or mutant arrestin-2 proteins. 48 h post-transfection the cells were fixed and stained with 4′,6-diamidino-2-phenylindole (*DAPI*). The slides were visualized, and images were acquired on an Olympus BX-61 fluorescence microscope.

## DISCUSSION

The data presented in this study reveal novel structural and functional roles for the interaction of arrestin-2 with $IP_6$. Here we show the crystal structure of arrestin-2 in complex with $IP_6$ and establish that two crystallographically identified $IP_6$-binding sites are required for $IP_6$-dependent arrestin-2 oligomerization *in vitro* and for arrestin-2 oligomerization in cells.

$IP_6$ binds in a highly electropositive surface on the C-domain of arrestin-2, making contacts with several lysine and arginine residues (Fig. 1, *B* and *E*). In addition, the crystal structure suggests a second $IP_6$-binding site on the N-domain of arrestin-2. This site is also highly electropositive, inviting highly negatively charged molecules such as $IP_6$ to bind (Fig. 1, *B* and *E*). The number of contacts between arrestin-2 and $IP_6$ at the N-domain are less extensive and would be predicted to be the weaker of the two binding sites. The biochemical data support this two-site model with the C-domain having ~20 times higher affinity for $IP_6$ than the N-domain.

The overall stoichiometry of arrestin-2 to $IP_6$ in the crystal and in lattice-based arrestin-2 oligomers is 1:1. However, at low arrestin-2 concentrations, as shown in Fig. 2, *B* and *C*, independent, sequential binding of $IP_6$ can be seen to the N-domain and the C-domain producing a form of arrestin-2 bound to two equivalents of $IP_6$. Both ITC and radiolabeled $IP_6$ binding assays established that the higher affinity binding event was saturable at 40–50 nM, whereas the lower affinity binding event was saturable at 0.9–2.6 $\mu$M. At arrestin-2 protein concentrations of 5–20 $\mu$M, $IP_6$ binding led to a quantitative shift in protein size. Consistent with the lattice model of $IP_6$-dependent oligomerization, $IP_6$ was incapable of inducing oligomerization of ND domain or CD domain mutants, whereas a mixture of the two proteins *trans*-complemented each other and produced an oligomer of a distinct size smaller than the $IP_6$-dependent wild type oligomer.

Of all the $IP_6$ binding assays performed, the ITC assay is the most complex because the initial protein concentration (10 $\mu$M, which declines to 8.4 $\mu$M over the course of the titration) was sufficient to promote $IP_6$-dependent oligomerization as $IP_6$ binds to the protein. Thus, the first binding event at 40 nM $IP_6$ is consistent with simple $IP_6$ binding to the C-domain. The second binding event, recorded at 2.6 $\mu$M by calorimetry, is likely to reflect half-saturation of $IP_6$ binding to the N-domain. However, if the C-domains are largely saturated by this point in the titration then, according to the lattice model, this 2.6 $\mu$M event is arrestin-2 polymerization where the N-domain site binds arrestin-2 already bound to $IP_6$ via the C-domain. Whereas the ultimate $IP_6$ stoichiometry of arrestin-2 polymerization is 1:1, by holding the protein concentration at 40 nM in the tritiated $IP_6$ binding assay, we were able to measure both $IP_6$ binding events at a protein concentration at which little oligomerization occurs.

Earlier Gaidarov *et al.* (2) using site-directed mutagenesis reported a high affinity phosphoinositide-binding site located on the C-domain of arrestin-3. They also determined the dissociation constants for a variety of phosphoinositides and inositol phosphates on binding to both arrestin-2 and -3. Of the ligands tested (phosphatidylinositol 4,5-bisphosphate, phosphatidylinositol 3,4,5-trisphosphate, inositol 1,4,5-trisphosphate, inositol 1,3,4,5-tetrakisphosphate, and $IP_6$), $IP_6$ displayed the highest affinity for arrestin with $K_d = 0.085$ $\mu$M in good agreement with the data presented here (2) (Fig. 2*A*). Mutation of this site impaired arrestin-3 recruitment to coated pits and effectively disrupted receptor endocytosis. *Drosophila* visual arrestin also contains a C-terminal domain phosphoinositide-binding site reported to interact strongly with $IP_6$ (13). Alteration of this site interfered with arrestin trafficking in photoreceptor cells effecting light adaptation. The role of the N-terminal domain in binding phosphoinositides is poorly understood. Although the N-terminal domain of arrestin-3 had been suggested to interact with $IP_6$, the nature and function of this interaction has not been characterized (2).

Our structural and biochemical data provide evidence for $IP_6$-mediated arrestin-2 oligomerization. The crystal lattice shows $IP_6$ mediating an interaction between the N-domain of one arrestin-2 molecule with the C-domain of a symmetry mate in a head to tail conformation (Fig. 3*A* and supplemental Fig. 3A). Studies have reported that arrestin-1 can form dimers and tetramers in solution (29, 34, 35). In fact, a head to tail dimer arrangement of arrestin-1 is the favored molecular architecture (35). The proposed oligomeric interfaces between our model and the arrestin-1 model are closely related. They both show similar parallel strand-strand (S6 and S11) interactions and a unique interclasping of rolled sheets between the N- and C-domains (35) where $IP_6$ is positioned in the arrestin-2 assembly (supplemental Fig. 3, A and B). The extensive chelating contacts provided by $IP_6$ are proposed to stabilize the arrestin-2 oligomer. Two truncated forms of arrestin-2, arrestin-2-(1–382) and arrestin-2-(1–393), have been suggested to form dimers (30). The reported models, unlike arrestin-1 and arrestin-2·$IP_6$, depict a tail (C-domain) to tail (C-domain) organization (supplemental Fig. 3C). This molecular interface is less extensive than the head to tail assembly with interactions occurring primarily through the S11-S12 and S15-S16 loop regions. Arrestin-2-(1–382) was reported to exist as a 4:1 mixture of monomer to dimers determined by gel filtration. In contrast, our structural model was tested using a number of protein sizing techniques: native gel electrophoresis, gel filtration, and analytical ultracentrifugation. Native gel electrophoresis revealed an $IP_6$-dependent gel

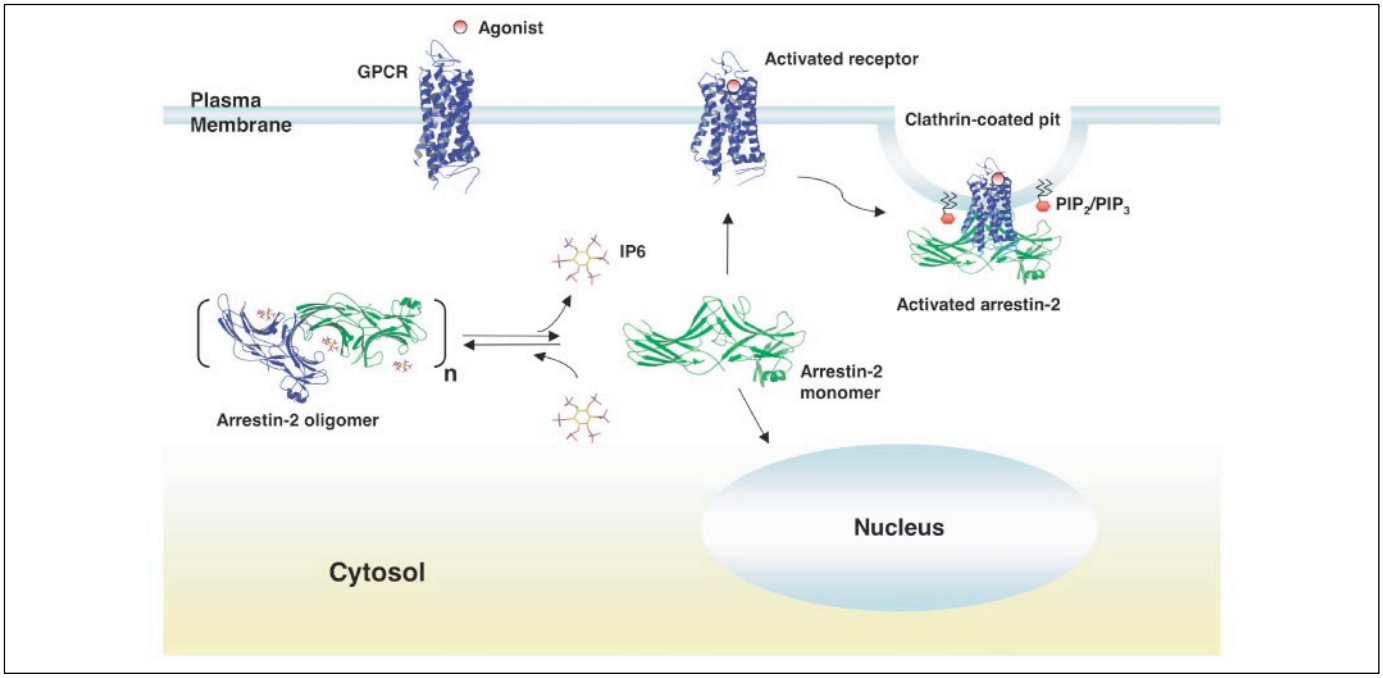


FIGURE 7. **Model for $IP_6$-dependent regulation of arrestin oligomerization and function.** Arrestin-2 oligomers, unable to bind receptors, function as a local store of inactive arrestin. The combination of arrestin-2 containing a low and high affinity site for $IP_6$ along with the changing level of free $IP_6$ within the cell would regulate the dissociation of arrestin oligomers and the movement of monomeric arrestin to activated receptors. Arrestin-2 oligomers are localized primarily in the cytoplasm enabling the mobilization of arrestin-2 rapidly to the membrane. Arrestin-2 monomers, however, are imported into the nucleus where their interaction with nuclear binding partners might be enhanced. *$PIP_2$*, phosphatidylinositol 4,5-bisphosphate; *$PIP_3$*, phosphatidylinositol 3,4,5-trisphosphate; *GPCR*, G protein-coupled receptor.

shift of arrestin-2 (Fig. 3*B*), whereas gel filtration and analytical ultracentrifugation demonstrated $IP_6$-dependent arrestin-2 oligomerization (Fig. 4, *A*, *C*, and *D*). Our data showed that arrestin-2 is able to self-associate in a manner that jointly depends on $IP_6$ and $IP_6$-binding sites.

In this study co-immunoprecipitation experiments demonstrated that both arrestin-2 and -3 can homo- and heteroassociate in COS-1 cells (Fig. 5, *A* and *D*). Storez *et al.* (31) also recently showed using bioluminescence resonance energy transfer assays that arrestin-2 and -3 can homo- and heteroassociate in COS-7 cells. These observations open up the possibility of arrestin-2 and -3 functioning together as a complex. The proteins could then either collectively or independently impart their unique functions in regulating or propagating signaling cascades (7). Importantly mutation of either $IP_6$-binding site in arrestin-2 effectively disrupted self-association while maintaining normal binding functions to endocytic and signaling molecules (Fig. 5, *A–C*). Overall the biochemical, biophysical, and cellular studies provided substantial evidence for an $IP_6$-induced arrestin-2 oligomerization.

Analogous to the arrestin-1 dimer, the crystal structure shows that arrestin-2 self-associates in the basal "inactive" conformation (Fig. 3*A*). The biological implications for this type of association might include regulating the amount of arrestin-2 available for activation in the cell (35). For example, this molecular architecture would create a local store of inactive arrestin where arrestin molecules would be available to dissociate and bind activated receptors. The low affinity binding site on arrestin-2 for $IP_6$ makes this an attractive model, enabling arrestin to quickly mobilize from cytosolic oligomers and function at the membrane. The $IP_6$-dependent head to tail arrestin-2 conformation would also block the receptor-binding site, preventing arrestin complexes from interacting with receptors. Consistent with the lattice model, both Palczewski *et al.* (17, 18) and Gaidarov *et al.* (2) have shown that $IP_6$ inhibits arrestin binding to light-activated, phosphorylated rhodopsin.

Nonvisual arrestins have been shown to differ in their subcellular localization (36, 37). Arrestin-3 has been reported to contain a classical leucine-rich nuclear export signal located on the C-domain that enables it to shuttle between the nucleus and cytoplasm in a leptomycin B-sensitive manner. Arrestin-2 lacks a nuclear export signal and therefore does not exhibit the leptomycin B effect. However, both arrestin-2 and -3 are actively imported into the nucleus (36, 37). In this study, we investigated the localization of wild type and $IP_6$ binding-defective arrestin-2 mutants in HEK293 cells. The co-immunoprecipitation experiments demonstrated that wild type arrestin-2 can self-associate and likely form oligomers in cells, whereas the $IP_6$ binding-defective mutants were unable to associate. The subcellular localization of these different arrestin-2 molecular arrangements was tested. Wild type arrestin-2 localized predominately in the cytoplasm, whereas the mutants displayed a more nuclear distribution (Fig. 6). These results suggest that arrestin-2 monomers have a more efficient nuclear import mechanism than the oligomeric wild type arrestin-2. Furthermore hetero-oligomerization between arrestin-2 and -3 could result in cytoplasmic retention of wild type arrestin-2 due to the nuclear export signal in arrestin-3 (31). The nuclear import of monomeric arrestin-2 could help to regulate the amount of free arrestin available in the cytoplasm for cellular functions and might also regulate the ability of arrestin-2 to interact with potential nuclear partners such as Mdm2 (36, 38).

Collectively the data presented in this study suggest a novel model of arrestin-2 regulation mediated by inositol hexakisphosphate (Fig. 7). The oligomeric state of arrestin-2 should depend on the concentration levels and availability of $IP_6$ within the cell. Although the regulation of $IP_6$ levels is not completely understood, a number of studies have made significant contributions in understanding $IP_6$ biosynthesis in mammalian cells. Fujii and York (39) have reported recently that overexpression of inositol polyphosphate kinase 2 and inositol polyphosphate kinase 1 increased $IP_5$ and $IP_6$ levels in Rat-1 cells. Frederick *et al.* (40) also has demonstrated that mouse cells deficient in inositol polyphosphate kinase 2 are disrupted in $IP_5$ and $IP_6$ synthesis, although $IP_6$ could still be detected albeit at reduced levels. Similarly Verbsky *et al.* (41) have

described the disruption of inositol 1,3,4,5,6-pentakisphosphate 2-kinase (also called 2-kinase and inositol polyphosphate kinase 1) in mice. They found that mouse embryonic fibroblasts heterozygous for the 2-kinase gene had decreased kinase activity, elevated levels of $IP_5$, and therefore reduced turnover to $IP_6$. In addition to 2-kinase, Verbsky *et al.* (42) showed inositol 1,3,4-trisphosphate 5/6-kinase and inositol 1,3,4,6-tetrakisphosphate 5-kinase are important enzymes in regulating cellular $IP_5$ and $IP_6$ levels. These findings demonstrate the complexity of $IP_6$ biosynthesis and suggest that multiple pathways and enzymes contribute to $IP_6$ generation. Cellular levels of $IP_6$ have been reported to be within 15–100 $\mu$M, clearly high enough to support arrestin-2 multimerization despite not all of this being freely available (14). Arrestin-2 oligomers, unable to bind receptors, would function as a local store of inactive arrestin (35). The combination of arrestin-2 containing a low and high affinity site for $IP_6$ along with the changing level of $IP_6$ within the cell may regulate the dissociation of the complex. We hypothesize that release of nonvisual arrestins from cytosolic multimers may be limiting for arrestin binding to activated receptors and for entry into the nucleus.

*Acknowledgments—We are grateful to Dr. Vsevolod V. Gurevich for providing purified arrestin-3, Dr. Henry N. Higgs for guidance with analytical ultracentrifugation, Dr. Charles P. Scott for help with isothermal titration calorimetry, and Dr. John Williams for helpful discussions. We are also grateful to Steve Luke for technical assistance. We thank the staff at beamline X25 at the National Synchrotron Light Source for technical support.*

**REFERENCES**

1. Pierce, K. L., and Lefkowitz, R. J. (2001) *Nat. Rev. Neurosci.* **2,** 727–733
2. Gaidarov, I., Krupnick, J. G., Falck, J. R., Benovic, J. L., and Keen, J. H. (1999) *EMBO J.* **18,** 871–881
3. Goodman, O. B., Jr., Krupnick, J. G., Santini, F., Gurevich, V. V., Penn, R. B., Gagnon, A. W., Keen, J. H., and Benovic, J. L. (1996) *Nature* **383,** 447–450
4. Kim, Y. M., and Benovic, J. L. (2002) *J. Biol. Chem.* **277,** 30760–30768
5. Laporte, S. A., Oakley, R. H., Zhang, J., Holt, J. A., Ferguson, S. S., Caron, M. G., and Barak, L. S. (1999) *Proc. Natl. Acad. Sci. U. S. A.* **96,** 3712–3717
6. Luttrell, L. M., Ferguson, S. S., Daaka, Y., Miller, W. E., Maudsley, S., Della Rocca, G. J., Lin, F., Kawakatsu, H., Owada, K., Luttrell, D. K., Caron, M. G., and Lefkowitz, R. J. (1999) *Science* **283,** 655–661
7. Lefkowitz, R. J., and Shenoy, S. K. (2005) *Science* **308,** 512–517
8. Shenoy, S. K., and Lefkowitz, R. J. (2005) *J. Biol. Chem.* **280,** 15315–15324
9. McDonald, P. H., Chow, C. W., Miller, W. E., Laporte, S. A., Field, M. E., Lin, F. T., Davis, R. J., and Lefkowitz, R. J. (2000) *Science* **290,** 1574–1577
10. Ge, L., Ly, Y., Hollenberg, M., and DeFea, K. (2003) *J. Biol. Chem.* **278,** 34418–34426
11. Roth, M. G. (2004) *Physiol. Rev.* **84,** 699–730
12. Beck, K. A., and Keen, J. H. (1991) *J. Biol. Chem.* **266,** 4442–4447
13. Lee, S. J., Xu, H., Kang, L. W., Amzel, L. M., and Montell, C. (2003) *Neuron* **39,** 121–132
14. Shears, S. B. (2001) *Cell. Signal.* **13,** 151–158
15. Sasakawa, N., Sharif, M., and Hanley, M. R. (1995) *Biochem. Pharmacol.* **50,** 137–146
16. Gaidarov, I., Chen, Q., Falck, J. R., Reddy, K. K., and Keen, J. H. (1996) *J. Biol. Chem.* **271,** 20922–20929
17. Palczewski, K., Pulvermuller, A., Buczylko, J., Gutmann, C., and Hofmann, K. P. (1991) *FEBS Lett.* **295,** 195–199
18. Palczewski, K., Rispoli, G., and Detwiler, P. B. (1992) *Neuron* **8,** 117–126
19. Lee, J. H., Jeong, S. M., Lee, B. H., Noh, H. S., Kim, B. K., Kim, J. I., Rhim, H., Kim, H. C., Kim, K. M., and Nah, S. Y. (2004) *J. Biol. Chem.* **279,** 9912–9921
20. Milano, S. K., Pace, H. C., Kim, Y. M., Brenner, C., and Benovic, J. L. (2002) *Biochemistry* **41,** 3321–3328
21. Kim, Y. M., Barak, L. S., Caron, M. G., and Benovic, J. L. (2002) *J. Biol. Chem.* **277,** 16837–16846
22. Parent, J. L., Labrecque, P., Orsini, M. J., and Benovic, J. L. (1999) *J. Biol. Chem.* **274,** 8941–8948
23. Otwinowski, Z., and Minor, W. (1997) *Methods Enzymol.* **276,** 307–326
24. Brunger, A. T., Adams, P. D., Clore, G. M., DeLano, W. L., Gros, P., Grosse-Kunstleve, R. W., Jiang, J. S., Kuszewski, J., Nilges, M., Pannu, N. S., Read, R. J., Rice, L. M., Simonson, T., and Warren, G. L. (1998) *Acta Crystallogr. Sect. D Biol. Crystallogr.* **54,** 905–921
25. Jones, T. A., Zou, J. Y., Cowan, S. W., and Kjeldgaard, M. (1991) *Acta Crystallogr. Sect. A* **47,** 110–119
26. Laskowski, R. A., MacArthur, M. W., Moss, D. S., and Thornton, J. M. (1993) *J. Appl. Crystallogr.* **26,** 283–291
27. Ford, M. G., Pearse, B. M., Higgins, M. K., Vallis, Y., Owen, D. J., Gibson, A., Hopkins, C. R., Evans, P. R., and McMahon, H. T. (2001) *Science* **291,** 1051–1055
28. Collins, B. M., McCoy, A. J., Kent, H. M., Evans, P. R., and Owen, D. J. (2002) *Cell* **109,** 523–535
29. Hirsch, J. A., Schubert, C., Gurevich, V. V., and Sigler, P. B. (1999) *Cell* **97,** 257–269
30. Han, M., Gurevich, V. V., Vishnivetskiy, S. A., Sigler, P. B., and Schubert, C. (2001) *Structure* (*Camb.*) **9,** 869–880
31. Storez, H., Scott, M. G., Issafras, H., Burtey, A., Benmerah, A., Muntaner, O., Piolot, T., Tramier, M., Coppey-Moisan, M., Bouvier, M., Labbe-Jullie, C., and Marullo, S. (2005) *J. Biol. Chem.* **280,** 40210–40215
32. Luttrell, L. M., Roudabush, F. L., Choy, E. W., Miller, W. E., Field, M. E., Pierce, K. L., and Lefkowitz, R. J. (2001) *Proc. Natl. Acad. Sci. U. S. A.* **98,** 2449–2454
33. DeFea, K. A., Vaughn, Z. D., O'Bryan, E. M., Nishijima, D., Dery, O., and Bunnett, N. W. (2000) *Proc. Natl. Acad. Sci. U. S. A.* **97,** 11086–11091
34. Imamoto, Y., Tamura, C., Kamikubo, H., and Kataoka, M. (2003) *Biophys. J.* **85,** 1186–1195
35. Schubert, C., Hirsch, J. A., Gurevich, V. V., Engelman, D. M., Sigler, P. B., and Fleming, K. G. (1999) *J. Biol. Chem.* **274,** 21186–21190
36. Wang, P., Wu, Y., Ge, X., Ma, L., and Pei, G. (2003) *J. Biol. Chem.* **278,** 11648–11653
37. Scott, M. G., Le Rouzic, E., Perianin, A., Pierotti, V., Enslen, H., Benichou, S., Marullo, S., and Benmerah, A. (2002) *J. Biol. Chem.* **277,** 37693–37701
38. Shenoy, S. K., McDonald, P. H., Kohout, T. A., and Lefkowitz, R. J. (2001) *Science* **294,** 1307–1313
39. Fujii, M., and York, J. D. (2005) *J. Biol. Chem.* **280,** 1156–1164
40. Frederick, J. P., Mattiske, D., Wofford, J. A., Megosh, L. C., Drake, L. Y., Chiou, S. T., Hogan, B. L., and York, J. D. (2005) *Proc. Natl. Acad. Sci. U. S. A.* **102,** 8454–8459
41. Verbsky, J., Lavine, K., and Majerus, P. W. (2005) *Proc. Natl. Acad. Sci. U. S. A.* **102,** 8448–8453
42. Verbsky, J. W., Chang, S. C., Wilson, M. P., Mochizuki, Y., and Majerus, P. W. (2005) *J. Biol. Chem.* **280,** 1911–1920
43. DeLano, W. L. (2002) *Pymol*, Version 0.97, DeLano Scientific, San Carlos, CA